Copper-hydrogen complexes in silicon

S. Knack* and J. Weber
University of Technology, D-01062 Dresden, Germany

H. Lemke and H. Riemann
Institute of Crystal Growth (IKZ), D-12489 Berlin, Germany
(Received 26 October 2001; published 4 April 2002)

Defect complexes of copper and hydrogen in silicon were studied in detail by deep-level transient spectroscopy. Floating-zone silicon, both *n* and *p* types, which had been copper doped during the growth, was hydrogenated by chemical etching. We determine the electrical parameters of substitutional copper and various copper-related deep levels. The concentration profiles after etching were measured and numerically fitted assuming a successive trapping of hydrogen atoms to substitutional copper. From our data we assign the Cu-related deep levels to different charge states of copper-hydrogen complexes containing one or two hydrogen atoms. For the CuH_1 defect we measured deep levels at $E_C-0.36$ eV and $E_V+0.54$ eV. The two levels at $E_C-0.25$ eV and $E_V+0.27$ eV we assigned to a CuH_2 complex. We also have evidence for a neutral complex containing three or more hydrogen atoms. In *p*-type silicon, the capture radii for hydrogen by the substitutional copper have been determined to be 0.3 nm for the first and second hydrogen atoms and 1.0 nm for a third hydrogen atom. In *n*-type material these values are found to be higher: 0.7 nm, 0.9 nm, and 1.8 nm, respectively.

DOI: 10.1103/PhysRevB.65.165203 PACS number(s): 61.72.Cc, 61.72.Ss, 66.30.Dn

I. INTRODUCTION

The interstitial species of copper and hydrogen are both fast diffusers in silicon, especially copper, which, to our best knowledge, has the highest diffusivity that has been measured in silicon.[1–3] Both can form neutral complexes with acceptors, such as B-H or B-Cu pairs, with the former showing a higher thermal stability.

Hydrogen has three charge states: negative, neutral, and positive. The Hubbard correlation energy is negative, so that the neutral charge state of hydrogen is not stable.[4] The positive and negative charge states have been identified by drift experiments in *n*-type and *p*-type silicon.[5,6] Interstitial copper, on the contrary, was believed to have no level in the band gap of silicon, being always positively charged for all values of the Fermi energy. A deep level found recently in *n*-type material has been tentatively assigned to the donor level of interstitial copper.[7]

While the solubility of copper at high temperatures is dominated by the interstitial species, it can also occupy the substitutional lattice site.[8,9] At room temperature, substitutional copper is immobile and can react with interstitial hydrogen to form defect complexes. For a number of different transition metals (such as Au, Ag, Pt, Pd, etc.) the defect complexes with hydrogen have been studied.[10–13] Most of the defects were investigated using deep-level transient spectroscopy (DLTS), but also electron-paramagnetic-resonance and Fourier-transform infrared studies have been performed for the cases of gold and platinum.[14–16] For platinum-hydrogen complexes, it could be shown that indeed the same defects were measured by the different techniques and the electrical, chemical, and structural information could be brought together to form a rather complete picture of the defect structure.

In this paper we present results from our work on copper-hydrogen complexes. Preliminary results were given in Ref. 17. Special emphasize is laid on the concentration profiles of the defects measured after hydrogenation. A detailed analysis allows us to obtain information about the nature of the defects and about the reaction kinetics. We discuss the mathematical model used for this analysis before we apply it to the case of copper and hydrogen.

II. SAMPLE MATERIAL AND EXPERIMENTAL METHODS

For our study we used floating-zone material of both *n*-type and *p*-type conductivities. Samples from different crystals were measured with the phosphorus or boron concentration of the order of 1×10^{14} cm^{-3} and 1×10^{15} cm^{-3}. A few micrograms of pure copper were dissolved in the volume of the silicon melt resulting in a concentration of the order of 1×10^{19} cm^{-3} in the melt. Due to the small segregation coefficient of copper in silicon, copper was incorporated into the solid crystal at a concentration of about 1×10^{15} cm^{-3}. This was confirmed by secondary ion-mass spectroscopy measurements on some of the samples. As expected from the precipitation behavior, the electrically active copper is only a small fraction (1×10^{13} cm^{-3}) of the total copper concentration.

Before measurement all samples were chemically etched. We used mixtures of $HF:HNO_3$ (1:6) or $HF:HNO_3:CH_3COOH$ (1:2:1 or 1:2:2), which remove the silicon material with different velocities. The etching rates were determined by measuring the wafer thickness before and after etching.

Schottky diodes were formed by thermal evaporation of either gold (for *n*-type material) or aluminum (for *p*-type material) contacts with diameters ranging from 1 to 3 mm. The Ohmic contacts consisted of an eutectic indium/gallium

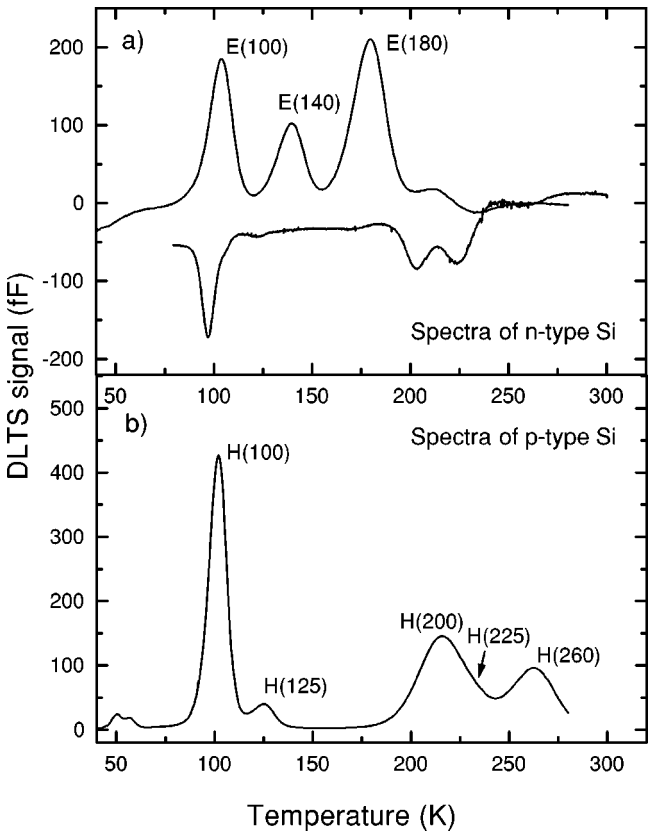

FIG. 1. DLTS and MCTS spectra of floating-zone Si:Cu. Spectra were measured at an emission time of 42 ms in DLTS and 50 ms in MCTS. (a) *n*-type material; (b) *p*-type material.

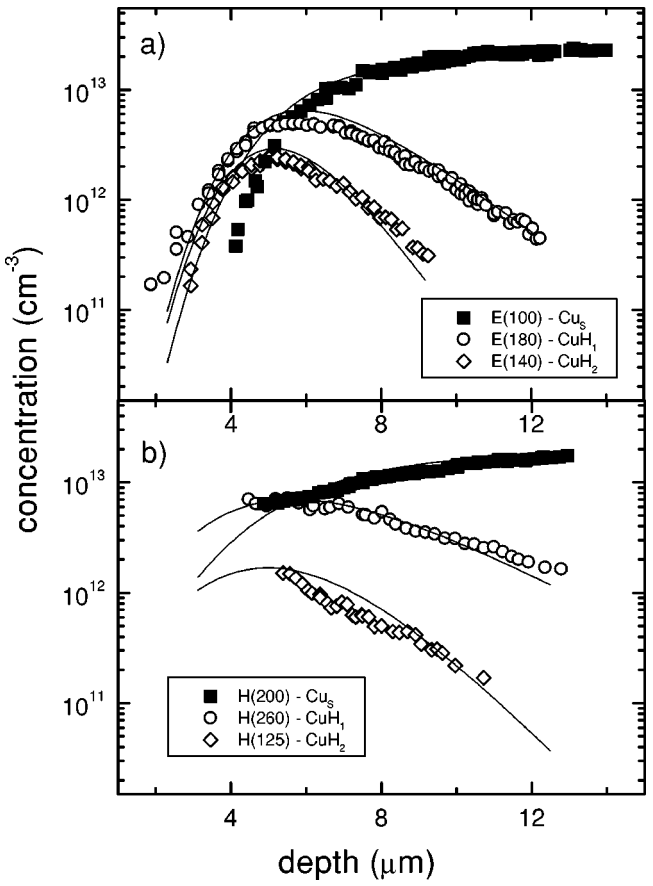

FIG. 2. Depth profiles of copper-related levels (a) in *n*-type silicon and (b) in *p*-type silicon.

alloy scratched onto the back surface.

Capacitance-voltage (*CV*) measurements were performed with an *LCR* meter at 1 MHz or 500 kHz. DLTS and minority-carrier transient spectroscopy (MCTS) experiments were performed on the Schottky contacts. For the DLTS and MCTS experiments two different cryostats were used, which could be cooled by liquid helium for DLTS and liquid N_2 for MCTS. The capacitance transients were analog filtered, whereby different filters (first to third order) could be used for signal processing. The MCTS measurements were done by backside illumination of the samples. In order to get spatially resolved concentration profiles for the measured deep levels, DLTS measurements at different voltages were performed. For the correct calculation of the concentrations the depth profiles of the free carriers as obtained by *CV* measurements were taken into account.

III. RESULTS

A. Deep levels

The DLTS and MCTS spectra measured in our *n*-type and *p*-type samples are shown in Fig. 1. The deep levels were labeled as shown in Fig. 1. Electron traps are indicated by an ''E'' and hole traps by an ''H'' followed by the approximate peak temperature for an emission time of 42 ms in DLTS and 50 ms in MCTS. Due to different correlation functions and pulse-repetition rates, not exactly the same emission-rate windows were realized in the DLTS and MCTS measurements. There are three dominant peaks in the DLTS spectrum of the *n*-type sample [E(100) to E(180)]. The depth profiles of the concentration of these levels are shown in Fig. 2 and discussed in detail in the next paragraph. The levels in the lower half of the band gap can be seen from the majority spectrum in *p*-type material as well as from the minority spectrum of the *n*-type sample.

Contrary to the DLTS measurements, the level H(260) can hardly be seen in the MCTS spectrum, which might indicate that the photocurrent and the hole capture coefficient of H(260) were too small to significantly fill the level. On the other hand, the levels H(200) and H(225) overlap more strongly in the DLTS spectrum because of the lower-order filter. H(225) can only be seen as a shoulder to H(200). Fitting the two overlapping peaks shows that H(225) is smaller relative to H(200) in the majority spectrum compared to the minority spectrum. The reason for this might be that H(200) is not completely filled in the MCTS experiment or that the formation of H(225) depends on the level of the Fermi energy and therefore differs between *n*-type and *p*-type materials.

The deep levels have previously been assigned to substitutional copper and copper complexes containing one or two hydrogen atoms. The peaks E(100), H(100), and H(200) are the three charge states of the isolated substitutional copper atom in silicon.[8,9] We assigned E(180) and H(260) to a CuH_1

TABLE I. Summary of defect properties: Level, activation energy, electron-capture cross section, barrier for thermally activated electron capture, hole capture cross section, level assignment, and radius of hydrogen capture.

Level	E_A (eV)	c_n ($cm^3\,s^{-1}$)	E_b (eV)	c_p ($cm^3\,s^{-1}$)	Assignment	r_H (nm)
E(100)	0.167(3)	3.2×10^{-10} (105 K)	0.025(3)	6.5×10^{-6} (105 K)	$Cu_S^{-/-}$	0.7
E(140)	0.254(4)	4.6×10^{-11} (143 K)	0.050(4)	7.0×10^{-6} (144 K)	$CuH_2^{-/-}$	0.9
E(180)	0.360(3)	7.5×10^{-11} (183 K)	0.050(4)	1.3×10^{-5} (185 K)	$CuH_1^{-/-}$	1.8
H(100)	0.207(4)			$2.4\times10^{-5}/8.9\times10^{-7}$ (97 K)	$Cu_S^{0/+}$	
H(125)	0.27(1)				$CuH_2^{-/0}$	1.0
H(200)	0.478(5)			2.9×10^{-7} (202 K)	$Cu_S^{-/0}$	0.3
H(260)	0.54(1)			1.4×10^{-7} (248 K)	$CuH_1^{-/0}$	0.3

defect and H(140) and H(125) to CuH_2.[17] This assignment stems from the analysis of the concentration profiles of the defects and is explained in the following paragraphs. The microscopic identity of H(225) still unknown.

The properties of the deep levels are summarized in Table I. The activation energies were determined from Arrhenius plots taking into account the standard T^2 correction for the temperature dependence of the exponential prefactor. In *n*-type samples we measured the activation energies for electron emission to be $E_a = 0.17$ eV for E(100) and 0.25 eV and 0.36 eV for E(140) and E(180), respectively. The cross sections for electron capture were measured by filling-pulse variations. All three levels show a slight temperature dependence of their capture behavior as shown in Fig. 3. Assuming a thermally activated capture over a barrier, we fitted the temperature dependence with an exponential function. This gives activation energies for the capture of approximately 0.025 eV [level E(100)] and 0.050 eV for both E(140) and E(180) (see Table I). These barriers fall within the range that has been measured for other transition-metal hydrogen complexes before.[18] The minority capture was also measured by filling the levels with a voltage pulse of fixed duration and then emptying the levels by minority-carrier capture with optical pulses of variable duration.

For the electrical fields that can be sustained in our low-doped material we found no field dependence of the emission rate. The levels do not show the Poole-Frenkel effect of Coloumb-attractive centers. On the contrary, our data for the magnitude and temperature variations of the cross sections are consistent with the interpretation that the levels are double acceptors, which are Coulomb repulsive. Level E(100) has been assigned to the double-acceptor state of substitutional copper before.[8] The similar behavior of the two levels E(140) and E(180) leads us to assign them to double-acceptor levels of the respective copper-hydrogen complexes.

The activation energies for the hole traps in the lower half of the band gap are also given in Table I. The measurements of the capture cross sections revealed two components for the level H(100). Another defect level is overlapping with the copper donor level. We were not able to obtain minority spectra or measure minority-carrier capture in the *p*-type samples. The minority carriers could not be injected into the space-charge region by optical backside excitation used in our MCTS experiments, because the minority-carrier diffusion length was too small.

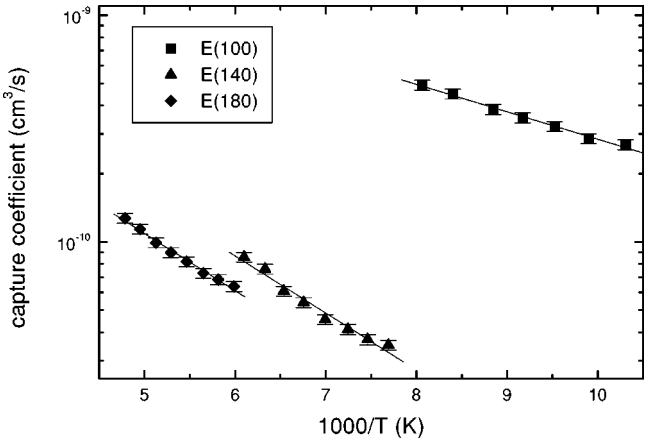

FIG. 3. Temperature dependence of the electron capture of the levels E(100), E(140), and E(180) in *n*-type samples.

B. Concentration profiles

As can be seen in Fig. 2, the substitutional copper defect is homogeneously distributed at greater depth and falls off towards the surface, in both *n*- and *p*-type samples. The missing concentration of isolated Cu_s near the surface is due to reactions of copper with other defects. The levels related to CuH_1 and CuH_2 are located near the surface and have an exponentially decreasing concentration at greater depth (Fig. 2). This is the expected behavior for complexes containing hydrogen that has been introduced by wet-chemical etching.[18,19] In *p*-type material, because of the strong overlap with the larger H(200) signal no profile for H(225) could be obtained. The nature of this level is not known up to now. In Fig. 2(b) only the profile measured for the level H(200) of substitutional copper is shown for better clarity. The profiles of levels H(100) and H(200) coincide deeper in the bulk material but show a significant difference in the near-surface region (see Fig. 4). While both profiles decrease towards the surface, the reduction in concentration of H(200) is more pronounced. From the assignment of the two levels to the donor and acceptor states of substitutional copper[8,9] one would expect completely identical profiles. There have been

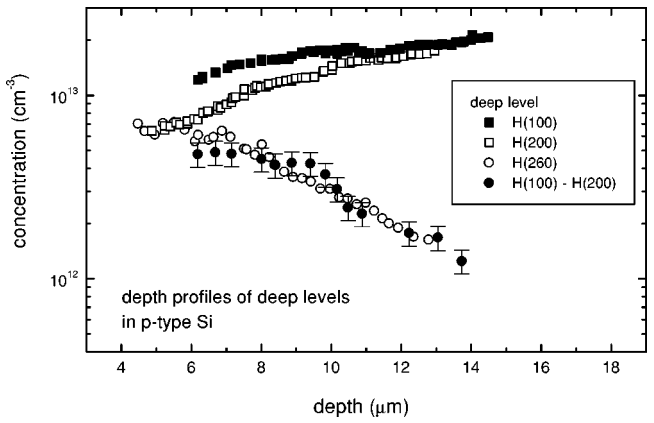

FIG. 4. Depth profiles of copper-related levels in silicon: profiles of levels H(100) and H(200), and their difference compared to the profile of H(260).

previous reports about this discrepancy in peak height between acceptor and donor levels, which had been tentatively related to an insufficient evaluation of the space-charge region at different temperatures. Our calculation of the profiles has taken this effect into account. We therefore can exclude space-charge effects as a reason. The difference in concentration is real and can only be found near the surface. From the capture measurements discussed in the previous paragraph we know that two defects must be contributing to the level H(100). When we compare the difference in concentration between H(100) and H(200) we get a profile that is very similar to the one measured for H(260) as is shown in Fig. 4.

Summing up the concentrations for E(100), E(140), and E(180) that account for all the defects containing copper, which can be measured in the upper half of the band gap, there is still a significant decrease in concentration in the near-surface region. The same is true in *p*-type samples where also copper is missing from the originally flat profiles. This means that there has to be at least one electrically passive complex with three or more hydrogen atoms. The existence of such defect complexes is supported by theoretical calculations. Molecular-dynamics simulations show that substitutional copper should be able to bind up to four hydrogen atoms in a stable configuration.[20,21]

C. Mathematical description

During the etching, hydrogen is incorporated into silicon and starts to diffuse until it is captured by a trap. The diffusion of hydrogen has to compete against the movement of the silicon surface which is caused by the etching, i.e., the hydrogen has to be able to outrun the surface movement. The hydrogen diffusion is described by the following partial differential equation:[19]

$$\frac{\partial H}{\partial t} = D_H \frac{\partial^2 H}{\partial x^2} + v \frac{\partial H}{\partial x} + \frac{eD_H}{kT} \frac{\partial}{\partial x}\left(H \frac{\partial \Phi}{\partial x}\right) - \frac{H}{\tau}. \quad (1)$$

Here H is the concentration of *free* hydrogen, D_H its diffusivity, and v denotes the velocity of the moving surface due to the etching. The third term takes into account the drift of the hydrogen due to an internal field. This is important in *p*-type material where the positively charged hydrogen efficiently passivates the boron acceptors resulting in an internal field due to the inhomogeneous concentration of electrically active acceptors:

$$e\Phi = kT \ln\left(\frac{N_D}{N_{D_0}}\right). \quad (2)$$

In *n*-type material the pairing between phosphorous donors and hydrogen is less efficient and the effect can be neglected. The fourth term describes the capture of hydrogen after a time τ by the traps in the material. It is assumed that the formed defect complexes are stable and no reemission of hydrogen occurs at room temperature. The capture time τ has to be calculated as follows:

$$\frac{1}{\tau} = 4\pi D_H \sum r_i N_i, \quad (3)$$

where the sum goes over the different traps for hydrogen. N_i is the concentration of the ith trap and r_i is the corresponding radius for hydrogen capture. The concentrations will change with time as part of the traps are already filled; the capture time τ will change accordingly.

In our case, the traps for hydrogen capture are the shallow doping species (boron or phosphorous) and substitutional copper which can form complexes with different numbers of hydrogen atoms. The defect complexes form according to

$$\frac{\partial CuH_i}{\partial t} = v \frac{\partial H}{\partial x} + 4\pi D_H (r_{i-1} CuH_{i-1} - r_i CuH_i) H. \quad (4)$$

Here again the motion of the silicon surface is taken into account by the first term on the right-hand side. The concentration of the complex containing i hydrogen atoms increases if hydrogen is captured by a defect containing $i-1$ hydrogen atoms ($i=0$ corresponds to the isolated, substitutional copper). The concentration decreases again if the defect itself captures hydrogen. This process stops at a maximum number of hydrogen atoms, when $r_{i_{max}}$ becomes zero.

Because the etchant constantly removes material from the silicon surface, the distribution of free and bound hydrogen does not penetrate deeper and deeper into the bulk but reaches a stationary profile after some time, when the velocities of diffusion and surface movement cancel out. The tails at greater depths of these stationary concentration profiles can be obtained from an analytical solution of the above equations. For larger x the approximation of $CuH_i \ll CuH_{i-1}$ holds true; i.e., only a small fraction of hydrogen was able to penetrate so far, so that the concentrations of the hydrogen complexes decrease with increasing i. Under these conditions the shallow doping can be seen as homogenous and the drift due to an internal electric field can be neglected. Furthermore, the second term on the right-hand side of Eq. (4) is dominated by the first term in the bracket and the second term can be neglected. Solving these simplified equations analytically yields

$$H \propto e^{-L_H/x}, \quad (5)$$

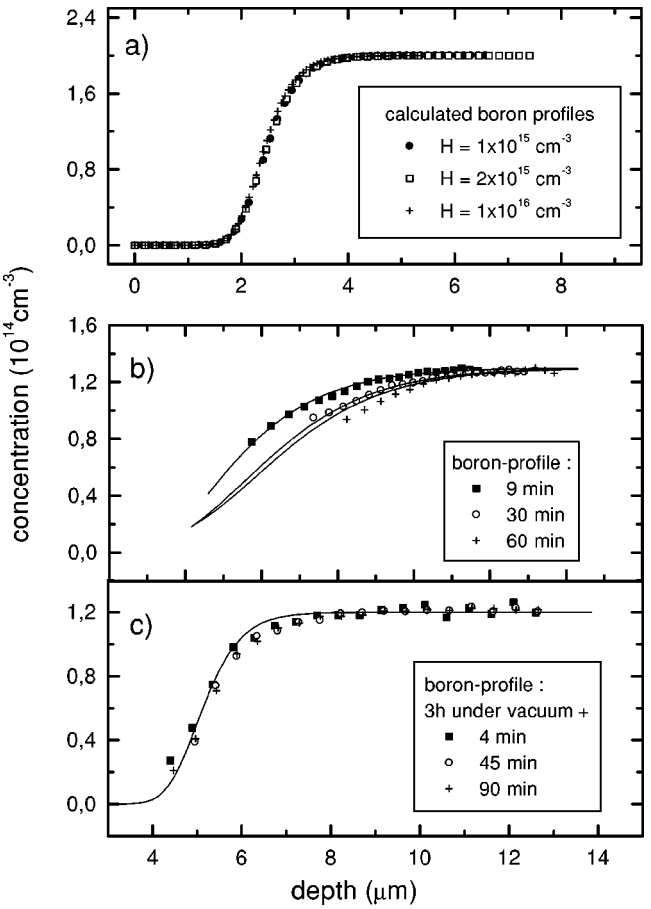

FIG. 5. Boron passivation by hydrogen diffusion: (a) calculated boron profiles for different values of H_0 and D_H, (b) time-dependent profiles from *CV* measurements directly after etching, and (c) stationary profile measured after storage under vacuum for three hours.

$$CuH_i \propto e^{-L_i/x}, \tag{6}$$

$$L_H = \left(\frac{v}{2D_H} + \sqrt{\frac{v^2}{4D_H^2} + \frac{1}{D\tau}} \right)^{-1}, \tag{7}$$

$$L_i = \frac{L_H}{i}. \tag{8}$$

The distribution of free hydrogen and hydrogen-related defects decreases exponentially with depth and the characteristic length is inversely proportional to the number of hydrogen atoms in the complex.

After the etch stop, the surface stops moving and no new hydrogen is incorporated into the sample. But the stationary distribution of free hydrogen starts to relax until all of the hydrogen is trapped. The effect of the continued diffusion can be monitored by repeated *CV* scans shortly after the etching of the samples as is shown in Fig. 5b. This relaxation is described by the same set of equations, with the difference that $v=0$ and the boundary conditions on the surface have to be chosen in such a way that the flux through the surface becomes zero.

D. Fitting procedure

In order to get a complete solution for the set of differential equations, they are transformed into discrete difference equations and solved numerically using the commercial MAPLE software. The free parameters of this system of equations are (1) the diffusivity D_H of hydrogen at room temperature, (2) the maximum hydrogen concentration H_0 close to the silicon surface, (3) the etching velocity v which was experimentally determined by measuring the sample thickness before and after etching, (4) the initial concentrations of hydrogen traps (here, the concentration of shallow dopants and substitutional Cu deeper in the bulk, where hydrogen could not penetrate so far, were taken from *CV* and DLTS measurements, respectively) and (5) the radii for hydrogen capture of the different traps.

Unfortunately, the solutions obtained from the calculations are not unique. The same final profiles can be obtained with different values for D_H if H_0 is also changed accordingly. Higher D_H implies lower H_0 and vice versa. This is demonstrated in the top panel of Fig. 5. The same boron profile was calculated for surface concentrations of hydrogen being 1×10^{15}, 2×10^{15}, and 1×10^{16} cm^{-3} when the hydrogen diffusivity was adjusted to be 2×10^{-10}, 1×10^{-10}, and 2.3×10^{-11} $\mathrm{cm}^2\,\mathrm{s}^{-1}$, respectively. In order to be able to distinguish between the different solutions additional experimental data on the initial hydrogen concentration is necessary.

The problem can be overcome by studying the time dependence of the relaxation after etching. The different combinations of D_H and H_0 lead to the same final concentration profiles, but the time after which these are reached differs significantly. Thus, the relaxation has to be monitored by a series of *CV* measurements shortly after etching. This can be best done in low-doped *p*-type silicon, where the capture time for hydrogen is comparatively small and the relaxation after etching is slow enough to be experimentally monitored. The result of such *CV* scans are shown in the middle panel of Fig. 5. The time for etching and formation of the Schottky diode was about 9 min. *CV* measurements at different times after etching show that the doping profile moves away from the surface as hydrogen is slowly diffusing in after the etching. For a correct evaluation it is important to take into account the difference between doping profile and majority-carrier profile. The profiles extracted from the *CV* scans have to be corrected for the majority-carrier diffusion in the region of inhomogenous doping. One should expect that at least, in principle, the applied field during *CV* measurements gives rise to an additional drift of the hydrogen in our *p*-type silicon samples. Yet, the measurement times for a *CV* scan were about 15 sec compared to the time scale of minutes for the observed movement of hydrogen. We checked two scans, one immediately after the other, and could detect no significant difference. Therefore, we conclude that this effect can be neglected.

Another sample was etched and then stored in vacuum at room temperature for three hours before the Schottky diodes were evaporated and the *CV* measurements performed (Fig. 5, bottom panel). The doping profile was essentially stable in

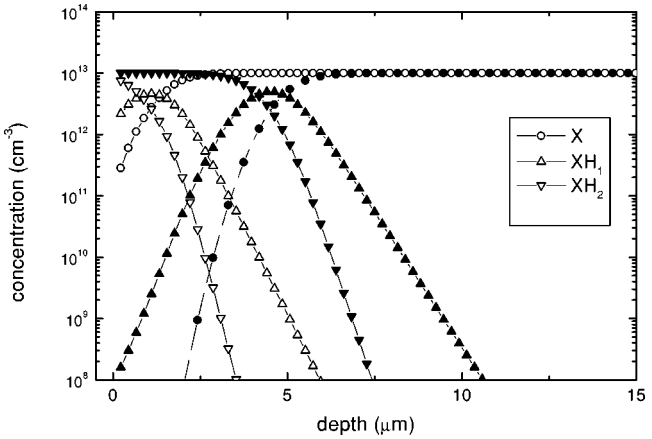

FIG. 6. Calculated profiles for a defect X and complexes with up to two hydrogen atoms XH_1 and XH_2. The open symbols are the profiles calculated for the time of the etch stop, while the final profiles after hydrogen relaxation are drawn with full symbols.

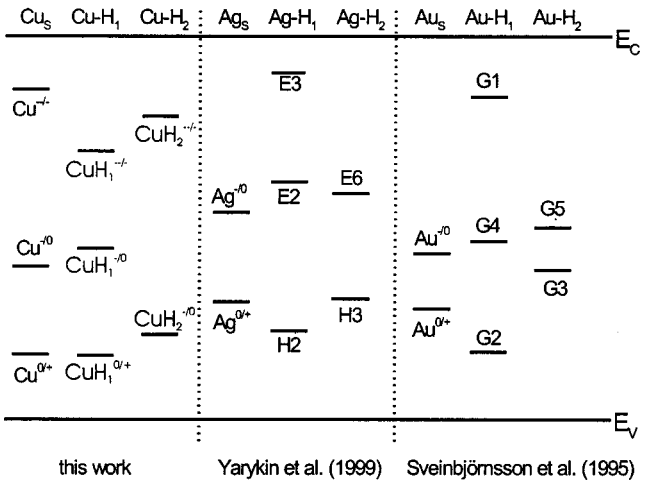

FIG. 7. Deep levels of the hydrogen complexes of the group-IB elements, copper, silver (Ref. 11), and gold (Ref. 10).

this sample and didn't move over the monitored period of 90 min. This shows that it is indeed the hydrogen that is responsible for the observed changes and not processes, which might be induced by the Al evaporation. Also, one can clearly see that the shape of the boron profiles is different for the two samples. This shows the effect of the Schottky contact on the hydrogen during diffusion. In the depletion region under the contact an additional field is present that makes the hydrogen drift deeper into the material. This effect does not exist, if the contact is evaporated at a time when no free hydrogen is left in the sample. From fits to the experimental data (solid lines in Fig. 5) we obtained a hydrogen diffusivity $D_H = 2.7 \times 10^{-10}$ cm^2 s^{-1} and a radius for hydrogen capture by boron of $r_B \approx 2.5$ nm.

With the obtained data for the hydrogen diffusion we can now try to fit the concentration profiles of the deep levels. It is important to note that for larger depth the calculations still predict an exponential behavior. The continued diffusion after the etching stopped changes the absolute values for the penetration depth L_H of hydrogen, but the relation $L_m/L_n = n/m$ which follows from Eq. (8) is still valid. Figure 6 shows deep-level profiles calculated for the time directly after etching (open symbols) and after the hydrogen distribution in the sample has completely relaxed (full symbols). As a result of the relaxation the profiles have broadened and moved further away from the surface, but the relation between the slopes for the exponential tail of the distributions has remained one to two. This means that the determination of the number of hydrogen atoms in a complex from the relative slopes as given previously[17,18] is not affected by the postetching diffusion. But of course, it has to be taken into account if correct values for the capture radii are to be extracted from the fits.

The results of the numerical fitting procedure are shown by the solid lines in Fig. 2. With the input for the hydrogen diffusion obtained from the CV measurements the remaining free parameters are the respective radii for hydrogen capture of the different defects. Under these restrictions the fits, while not being perfect, agree reasonably well with the experimental curves. In n-type material we extracted values of $r_{Cu} = 0.7$ nm, $r_{CuH_1} = 0.9$ nm, and $r_{CuH_2} = 1.8$ nm for the capture of hydrogen by Cu_S, CuH_1, and CuH_2, respectively. We want to stress the point that the profiles can only be fitted if we assume that a complex with three hydrogen atoms is formed (i.e., $r_{CuH_2} \neq 0$). The fits to the concentration profiles in our p-type samples give us the following results: $r_{Cu} = 0.3$ nm, $r_{CuH_1} = 0.3$ nm, and $r_{CuH_2} = 1.0$ nm. We estimate the margin of error for our fitting parameters within our model to be about 10%.

IV. DISCUSSION

The energy levels in the silicon band gap of substitutional copper and its hydrogen complexes are shown in Fig. 7 together with the respective levels of the other group-IB elements, silver and gold. In the so-called vacancy model[22] the electrical properties of substitutional transition metals are derived from the single silicon vacancy. The similarities of the substitutional transition metals have been found to translate to the hydrogen complexes.[13] The double-acceptor level could only be measured for copper; in the case of gold and silver it must be within the conduction band of silicon. For copper, silver, and gold, three levels are assigned to the complex containing one hydrogen atom and two levels are assigned to the complex with two hydrogen atoms. Also, the existence of an electrically passive complex containing three or more hydrogen atoms has been inferred in all cases.[10,11] The electrical levels of the three elements can thus be completely passivated by three hydrogen atoms.

Our value for the hydrogen diffusivity, $D_H = 2.7 \times 10^{-10}$ cm^2 s^{-1}, is close to values extrapolated from high-temperature measurements.[23] The diffusivity of hydrogen has been measured between 135 K and 1473 K by various methods. The measured values at room temperature range from 1×10^{-11} to 3×10^{-10} cm^2 s^{-1}.[24,27] Our result is at the upper limit of this range which has been the case before in studies using wet-chemical etching for hydrogen incorporation.[25] Lower values are often found, because what is actually ob-

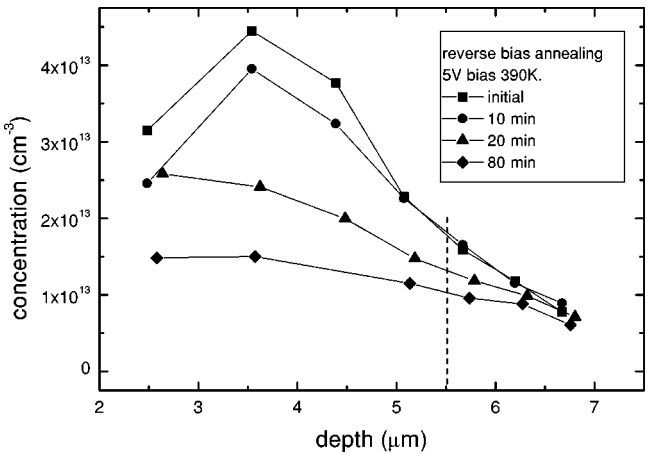

FIG. 8. Profiles of the CuH_2 defect after reverse bias annealing at 390 K and 5 V for different times. The width of the depletion region during reverse bias annealing is marked by the dashed line.

served is a trap-limited diffusion with an effective diffusivity, which is lower than the intrinsic value for D_H. The radius for hydrogen capture by boron was determined to be 2.5 nm in this work which is somewhat lower than the 4.0 nm obtained from drift experiments in *p*-type silicon.[26] The value for $H_0 = 9 \times 10^{14}$ cm^{-3} should be interpreted not as a surface concentration but rather as the volume concentration of free hydrogen away from the reaction zone where the chemical reactions during etching take place.

Compared to the capture by boron, hydrogen is less effectively bound to the substitutional copper, as is seen from the lower capture radii. The captures to the substitutional Cu and to the CuH_1 center with $r_H = 0.3$ nm in both cases are rather weak. The values suggest the interaction of the positively charged hydrogen with a neutral center. After the hydrogen capture, in order to stay neutral, the center has to capture an electron (i.e., a minority carrier). The increase in capture radius for the third hydrogen bound to copper ($r_H = 1.0$ nm) might be due to a more efficient minority capture. Another possible explanation might be that the capture of a third hydrogen becomes more efficient due to a somewhat higher lattice strain of the CuH_2 defect. The same trend of increasing capture radius is also seen in *n*-type material.

For a discussion of our data on the hydrogen capture, one has to bear in mind that interstitial hydrogen in silicon has a negative Hubbard correlation energy *U*, with the donor state lying 0.16 eV below the conduction band and the acceptor level being at midgap.[4,27] This means that in *p*-type silicon, hydrogen should occupy only the positive charge state, while in moderately *n*-type material, like was used in our experiments, hydrogen should be partly positively charged and partly negative. The Fermi level at room temperature in our samples is about 0.3 eV from the valence band or the conduction band in the *p*-type and *n*-type materials, respectively. The higher, more efficient capture of hydrogen to copper and the formed copper-hydrogen complexes in *n*-type material might be due to the positively charged fraction of the hydrogen, which is attracted to the more negative charge states of the defects occupied at this Fermi level. In *p*-type material, hydrogen is only positively charged and binds less effectively to the more positive charge states of the copper-related defects. This analysis is also supported by the fact that the CuH_2 defect in *n*-type silicon is less stable when annealed under a reverse bias, i.e., when the level in the upper half of the gap is not occupied by electrons. This is shown in Fig. 8: the concentration of the defect decreases only in the region where the level is unoccupied due to the applied voltage, while it stays virtually constant outside the space-charge region (the width of the depletion region during reverse bias annealing is marked by the dashed line).

About the level H(225) not much is known. The overlap with the higher peak H(200) in the DLTS spectra is too strong to allow for accurate measurements or depth profiling. The level can be seen better in our MCTS spectra. Depth profiling with MCTS is, in principle, possible, but needs more favorable conditions than met in our samples. While no assignment can be proposed for H(225) it seems to be related to copper and hydrogen, as it is not found in other samples containing no or other transition metals.

V. SUMMARY

In addition to the three levels of substitutional copper we found six more deep levels in our Cu-doped and hydrogenated silicon samples. Four levels could be assigned to different charge states of the complexes CuH_1 [E(180), H(260)] and CuH_2 [E(140), H(125)] by studying their electrical properties and concentration profiles. The second signal under the H(100) peak is tentatively assigned to a third charge state of CuH_1. The existence of one or more electrically passive complexes with higher numbers of hydrogen is indirectly derived from an analysis of the concentration profiles of the defects.

ACKNOWLEDGMENTS

The technical assistance of B. Köhler is gratefully acknowledged. This work was supported by the Deutsche Forschungsgemeinschaft under Project No. WE 1319/9-1.

*Electronic address: steffen.knack@physik.tu-dresden.de

[1] R. N. Hall and J. H. Racette, J. Appl. Phys. **35**, 379 (1964).
[2] J. D. Struthers, J. Appl. Phys. **27**, 1560 (1956).
[3] A. Mesli and T. Heiser, Phys. Rev. B **45**, 11 632 (1992).
[4] N. M. Johnson, C. Herring, and C. G. Van de Walle, Phys. Rev. Lett. **73**, 130 (1994).
[5] T. Zundel and J. Weber, Phys. Rev. B **39**, 13 549 (1989).
[6] J. Zhu, N. M. Johnson, and C. Herring, Phys. Rev. B **41**, 12 354 (1990).
[7] A. A. Istratov, C. Flink, H. Hieslmair, E. R. Weber, and T. Heiser, Phys. Rev. Lett. **81**, 1243 (1998).
[8] H. Lemke, Phys. Status Solidi A **95**, 665 (1986).
[9] S. D. Brotherton, J. R. Ayres, H. W. van Kesteren, and F. J. A. M. Greidanus, J. Appl. Phys. **62**, 1826 (1987).

[10] E. Ö. Sveinbjörnsson and O. Engström, Phys. Rev. B **52**, 4884 (1995).
[11] N. Yarykin, J.-U. Sachse, H. Lemke, and J. Weber, Phys. Rev. B **59**, 5551 (1999).
[12] J.-U. Sachse, E. Ö. Sveinbjörnsson, W. Jost, J. Weber, and H. Lemke, Phys. Rev. B **55**, 16 176 (1997).
[13] J.-U. Sachse, E. Ö. Sachse, N. Yarykin, and J. Weber, Mater. Sci. Eng., B **B58**, 134 (1999).
[14] M. Höhne, U. Juda, Yu. V. Martynov, T. Gregorkiewicz, C. A. J. Ammerlaan, and L. S. Vlasenko, Phys. Rev. B **49**, 13 423 (1994).
[15] S. J. Uftring, M. Stavola, P. M. Williams, and G. D. Watkins, Phys. Rev. B **51**, 9612 (1995).
[16] M. J. Evans, M. Stavola, and M. G. Weinstein, and S. J. Uftring, Mater. Sci. Eng., B **B58**, 118 (1999).
[17] S. Knack, J. Weber, and H. Lemke, Physica B **273-274**, 387 (1999).
[18] J.-U. Sachse, J. Weber, and E. Ö. Sveinbjörnsson, Phys. Rev. B **60**, 1474 (1999).
[19] O. V. Feklisova and N. A. Yarykin, Semicond. Sci. Technol. **12**, 742 (1997).
[20] S. K. Estreicher, Phys. Rev. B **60**, 5375 (1999).
[21] S. K. Estreicher (private communication).
[22] G. D. Watkins, Physica B & C **117&118**, 9 (1983).
[23] A. van Wieringen and N. Warmholtz, Physica (Amsterdam) **22**, 849 (1956).
[24] M. Stavola in *Properties of Crystalline Silicon*, edited by R. Hull (INSPEC, London 1999), Chap. 9.8, p. 511.
[25] A. J. Tavendale, A. A. Williams, and S. J. Pearton, Mater. Res. Soc. Symp. Proc. **104**, 285 (1988).
[26] T. Zundel and J. Weber, Phys. Rev. B **39**, 13 549 (1989).
[27] C. Herring, N. M. Johnson, and C. G. Van de Walle, Phys. Rev. B **64**, 125209 (2001).